KRONOS FUSION ENERGY

PAPER 2.46 · THE KRONOS 2026 SERIES

# *First-Principles Near-Neutral Low-Activation Refractory Alloys for Fusion Plasma-Facing Components: Formation-Energy Screening and Entropy-Stabilized Composition-of-Matter Design*

Structural and plasma-facing alloys that activate little and clear their radiological classification within a human lifetime are a hard requirement for a compact fusion breeder…

Read it live — 3-D model · physics validator · film series

BY P I FORD AND G L KULCINSKI

2026 · EDITORIAL EDITION

THE OFFICIAL RECORD

# What this document is, and how to read its numbers

This is a combined editorial. It gathers, in one volume, the two design studies Kronos Fusion Energy released in 2026 — a compact spherical-tokamak tritium/helium-3 breeder and a deuterium–helium-3 tandem-mirror generator — together with the intellectual-property estate, the people, and, in the internal edition, the full commercial case. The scientific text is the same text that appears in the arXiv preprints and the journal submissions; the editorial adds the apparatus a reader needs to hold the whole program at once, and nothing in the physics is altered to fit it.

## THE HONESTY STANCE IS THE ASSET

Every headline quantity carries an **evidence class** — DERIVED RECOMPUTED MEASURED REQUIREMENT — and, where a number is a modelled extrapolation rather than a demonstrated value, it is labelled as such and its downside is shown next to it. Several quantities in the underlying corpus moved after first publication; where a value has been withdrawn or restated, the record says so plainly. This is deliberate: a diligence team will find the load-bearing assumptions, so the document surfaces them first.

## TWO EDITIONS

This volume is issued in two editions. The **public edition** (light) carries the physics and the design only — no dollar, price, or per-kilogram figure appears anywhere in it. The **internal edition** (dark) adds the economics, the funding architecture, and the defense-commercial analysis, and is marked *Confidential* accordingly; it is not for public distribution. Where the commercial case rests on a modelled assumption rather than a demonstrated one, it is labelled as such and its downside is shown alongside it, on the same terms as the physics.

| | |
|---|---|
| TITLE | The Kronos Fleet — Hyperion · Aegis · MetroVolt: A Combined Design & Commercialization Study |
| AUTHOR | Priyanca Ford, Founder & CEO, on behalf of Kronos Fusion Energy |
| EDITION | 2026 Combined Editorial · first issue |
| COMPANION WORKS | The five-paper arXiv drop — (1) Breeder, (2) Burner, (3) REBCO magnet & tape, (4) Direct Energy Conversion, (5) AI/ML/Quantum control — with matching numbered Zenodo deposits, plus the IOP journal and IAEA-FEC submissions. Patents were filed before the drop. |
| NAMING | Hyperion = the breeder; Aegis (defense) and MetroVolt (data-center) = one generator in two housings. Internal mode letters (D1, L) do not appear on public surfaces. |
| STATUS | Conceptual design & simulation study. Nothing herein is a construction commitment. |

HOW TO READ THIS VOLUME

# The fleet at a glance, and the way its numbers are marked

This volume opens with *Orientation*, presents the five research papers as a bound sequence, and closes with the *Apparatus*. *Foundations* sets out the three general results both machines rest on. *Paper One* is the Hyperion breeder; *Paper Two* the Aegis / MetroVolt generator; *Papers Three, Four and Five* are the enabling science — high-field REBCO magnets and tape, direct energy conversion, and the AI / ML / quantum control stack. A *Digital Twin & 3-D Model* part follows, then the *Environmental* profile. The *Economics* and levelized cost and the *Business Case* and diligence record appear in the internal edition only; the *Simulations* proof record and the Apparatus — patent portfolio, team, limitations, and sources — close both editions.

## THE FLEET AT A GLANCE

| | HYPERION | AEGIS | METROVOLT |
|---|---|---|---|
| **Role** | Strategic-isotope foundry | Defense installation power | Campus power |
| **Machine** | **Spherical tokamak** | **Tandem mirror** | **Tandem mirror** |
| **Fuel** | Deuterium–tritium | Deuterium–helium-3 | Deuterium–helium-3 |
| **Delivers** | Tritium · $^{3}$He · 14 MeV n | Resilient installation power | Firm campus power |
| **Physics bar** | **Fusion gain only** | Closure (gates named) | Closure + lunar $^{3}$He |
| **In the fleet** | Breeds the fuel | Proves the generator | Commercial destination |

## HOW THE NUMBERS ARE MARKED

Every headline quantity carries an evidence class — DERIVED from first principles, RECOMPUTED from raw data, MEASURED in hardware, or a REQUIREMENT yet to be met. Financial figures carry a case label and are confined to the internal (confidential) edition. Values that moved after first publication are shown as withdrawn or restated rather than quietly changed. A capability you can evaluate is one whose limits are on the page.

ABSTRACT

# First-Principles Near-Neutral Low-Activation Refractory Alloys for Fusion Plasma-Facing Components: Formation-Energy Screening and Entropy-Stabilized Composition-of-Matter Design

Structural and plasma-facing alloys that activate little and clear their radiological classification within a human lifetime are a hard requirement for a compact fusion breeder and the natural home of composition-of-matter design. We report a first-principles screen of refractory multi-principal-element alloys for the first-wall, divertor, breeder-blanket, and direct-energy-converter (DEC) electrode roles of the Hyperion compact spherical-tokamak breeder (design point $Q = 3.076$, $P_{\mathrm{fus}} = 85.04\,MW$, $I_p = 9.66\,MA$, negative triangularity $\delta = -0.30$, $B_0 = 8\,T$, elongation $\kappa = 2.0$, $R_0 = 1.20\,m$, aspect ratio $A = 2.5$, centrepost peak field 16.84 T), where the first wall accumulates 18.85  per full-power year. A machine-learned interatomic potential (CHGNet) screens a $7500$-composition space and returns eight leads that we confirm by plane-wave density-functional theory (DFT; Quantum ESPRESSO, PBE) on special-quasirandom-structure (SQS) cells. The confirmed lead compositions are *near-neutral* in formation energy relative to their body-centred-cubic elemental references: the divertor alloy $Cr_1Ta_5Ti_3V_3W_4$ at $+0.015\,\mathrm{eV/atom}$ (two independent codes agree, $+0.0147$ and $+0.016$), the first-wall alloy $Cr_1Ta_4Ti_5V_3W_3$ at $+0.007$, an equiatomic W–Ta–V–Ti refractory high-entropy candidate at $+0.003$, and a blanket alloy at $+0.021\,\mathrm{eV/atom}$; a tantalum-free sub-family chosen to remove the long-lived activation tail spans $-0.002$ to $-0.015\,\mathrm{eV/atom}$. We show that once the ideal configurational mixing entropy is included, every lead has a negative Gibbs mixing free energy ($\Delta G_{\mathrm{mix}} \approx -0.11$ to $-0.12\,\mathrm{eV/atom}$ at 1000 K)—these are entropy-stabilized single-BCC candidates, with valence-electron concentrations of $4.88$–$5.31$ deep inside the BCC solid-solution window—while being enthalpically metastable-to-marginal rather than deeply stable single phases. We therefore state the invention basis honestly: it is the entropy-stabilized design-and-processing method that realizes and retains these low-activation compositions, not an intrinsic-enthalpy-stability claim. The screen uses a coarse SQS cell; a dense-cell confirmation is carried openly as a second wave, and no composition is presented here as a validated stable phase.

Open-access deposit (code & data, CC BY 4.0): DOI 10.5281/zenodo.22645744 · Zenodo community *kronos_fusion_energy*. Explore it live: interactive 3-D model · physics validator.

**Keywords:** low-activation alloys refractory high-entropy alloys density-functional theory formation energy special quasirandom structures machine-learned interatomic potentials fusion plasma-facing components

CONTENTS

# Table of Contents

NOMENCLATURE

# Symbols, units, and the names of things

| | |
|---|---|
| $Q$ | plasma (fusion) gain, $P_{fus}/P_{aux}$ |
| $Q_E$ | engineering gain, net electric out / recirculating in |
| $H_{98}$ | confinement enhancement over the IPB98(y,2) scaling |
| $Z_{eff}$ | effective ion charge |
| $c_{ee}$ | electron–electron bremsstrahlung leading coefficient, 2.120022 (exact) |
| $\tau_E$ | energy confinement time |
| $I_p$ | plasma current |
| $R_0, a$ | major radius, minor radius |
| $\kappa, \delta$ | elongation, triangularity |
| $\beta_N$ | normalized plasma beta (Troyon-normalized) |
| *TBR* | tritium breeding ratio |
| *DEC* | direct energy conversion |
| *CF* | plant capacity factor (availability) |
| *FOAK / NOAK / BOAK* | first / $n^{th}$ / best of a kind |
| *Hyperion* | the ST breeder (internal: Mode D2) |
| *Aegis* | the generator, defense/installation housing (internal: Mode M) |
| *MetroVolt* | the generator, data-center housing (Mode M) |

low-activation alloys; refractory high-entropy alloys; density-functional theory; formation energy; special quasirandom structures; machine-learned interatomic potentials; fusion plasma-facing components

§ 1

# Introduction

## WHY LOW-ACTIVATION REFRACTORY ALLOYS, AND WHY NOW

A compact fusion breeder that runs on a deuterium–tritium plasma exposes its plasma-facing components (PFCs) and first-wall structure to a 14.1 MeV neutron spectrum. Two consequences dominate materials selection. First, the neutrons displace lattice atoms; at the Hyperion first wall the displacement rate is 18.85  per full-power year, and each displacement cascade seeds the microstructural evolution —voids, bubbles, dislocation loops, and precipitation—that limits component life [1,2]. Second, transmutation and neutron capture convert the constituent elements into radioactive daughters, some of which are long-lived; the resulting inventory sets whether a decommissioned component can be cleared or must be managed as long-lived waste on a geological timescale [3,4]. A fusion system whose waste is to clear within a human lifetime must therefore be built, wherever the neutron flux is significant, out of *low-activation* elements combined so that no long-lived activation product accumulates [5,2].

The classical low-activation palette for fusion structure is narrow: reduced-activation ferritic–martensitic (RAFM) steels [6], vanadium alloys [7], silicon carbide composites, and, for the highest-flux surfaces, tungsten and its alloys [8]. Each element must be chosen not only for its mechanical and thermal performance but for the half-lives of its transmutation products: niobium (producing 94Nb), molybdenum, nickel, cobalt, and—for the divertor—rhenium, are the elements whose activation tails frustrate clearance. The design problem is combinatorial: the requirement is a single-phase, mechanically robust, refractory solid solution whose constituent set is restricted to activation-benign elements. This is precisely the territory of refractory high-entropy alloys (HEAs) [9,10,11]: multi-principal-element body-centred-cubic (BCC) solid solutions stabilized in part by configurational entropy, several of which have shown outstanding radiation tolerance [12] and have been fabricated for fusion PFC use [13].

## PRIOR ART: FROM HUME-ROTHERY RULES TO FIRST-PRINCIPLES AND MACHINE-LEARNED SCREENING

Phase selection in multicomponent alloys has historically been guided by empirical parameters: the valence-electron concentration (VEC) that discriminates BCC from FCC solid solutions [16], the atomic-size mismatch $\delta_r$ and mixing enthalpy $\Delta H_{\text{mix}}$ that bound single-phase formation [17], and the entropy–enthalpy competition that names the HEA class [14,15]. These rules are fast but coarse. The quantitative ground truth for phase stability is the density-functional-theory (DFT) formation energy [18,19], which for a disordered alloy is most economically evaluated on a special-quasirandom structure (SQS) [24,25] that reproduces the pair- and multi-site correlation functions of the random solid solution in a small periodic cell. DFT, however, is expensive, so the modern practice is to screen a very large composition space with a fast surrogate—a machine-learned interatomic potential (MLIP) [26,27]—and confirm only the leads at the DFT level. This MLIP-screen/DFT-confirm strategy is now standard in computational alloy discovery and is the backbone of the present work.

## CONTRIBUTION

We apply an MLIP-screened, DFT-confirmed, activation-filtered pipeline to the specific structural roles of the Hyperion breeder and its companion tandem-mirror burner's direct-energy converter. Our contributions are:

A formal statement of the coupled screening problem—electronic-structure ground state, SQS ensemble average, mixing free energy, and the activation and displacement constraints—as a set of governing equations (§2).
A GPU-accelerated computational campaign (§3) that screens $7500$ candidate compositions by MLIP and confirms eight leads by plane-wave DFT on SQS cells, with two independent plane-wave codes agreeing on the divertor lead.
The central quantitative result (§4): the confirmed leads are *near-neutral* in formation energy ($-0.015$ to $+0.021\,\mathrm{eV/atom}$), a result that refutes an earlier spurious $-0.172\,\mathrm{eV/atom}$ screen value and re-bases the intellectual property from intrinsic enthalpy stability onto the entropy-stabilized processing method.
A demonstration that the ideal configurational mixing entropy drives every lead to a negative Gibbs mixing free energy at service temperature, with valence-electron concentrations placing all leads inside the single-BCC window—the physical basis for calling these entropy-stabilized single-phase candidates. enumerate
The design point, the displacement rate, and the activation waste-class behaviour are frozen anchors of the Kronos physics de-risking programme; the breeder platform that defines them is described in the companion platform paper [33], its PFC lifetime under 14 MeV loading in [34], its component activation and waste-class routing in [35], and the plasma-material erosion budget in [36]. The MLIP-to-activation pipeline is developed at length in [37], the radiation-tolerant HEA processing route in [38], the tantalum- and rhenium-free family in [39], and the correlated-electron chemistry beyond DFT in [40].

§ 2

# Governing equations and the formal screening problem

## ELECTRONIC-STRUCTURE GROUND STATE

The primitive quantity is the total energy of a candidate supercell in its electronic ground state. Within Kohn–Sham DFT [18,19] the interacting many-electron problem is mapped onto non-interacting particles moving in an effective potential:

$$\left[-\frac{\hbar^2}{2m}\nabla^2 + V_{\text{ext}}(r) + V_H[n](r) + V_{xc}[n](r)\right]\phi_i(r) = \varepsilon_i\,\phi_i(r),$$

with the electron density and the Hartree potential closing the self-consistency loop,

$$n(r) = \sum_i^{\text{occ}} \left|\phi_i(r)\right|^2, \qquad V_H[n](r) = e^2 \int \frac{n(r')}{|r - r'|}\,\mathrm{d}^3 r',$$

and the exchange–correlation potential $V_{xc} = \delta E_{xc}[n]/\delta n$ taken in the Perdew–Burke–Ernzerhof (PBE) generalized-gradient approximation [20]. The total energy $E[n]$ is evaluated on a plane-wave basis with pseudopotentials; Brillouin-zone integrals use a Monkhorst–Pack mesh [21], and the atomic positions and cell shape are relaxed by variable-cell BFGS to the force/stress ground state.

## FORMATION ENERGY AND THE SQS ENSEMBLE AVERAGE

Phase stability of a candidate composition is screened by the formation energy per atom relative to the elemental references in their equilibrium (here BCC) structures,

$$E_f = \frac{1}{N}\left(E_{\text{alloy}} - \sum_i x_i\,E_i^{\text{bulk}}\right), \qquad \sum_i x_i = 1,$$

where $N$ is the number of atoms in the cell, $x_i$ the mole fraction of species $i$, and $E_i^{\text{bulk}}$ the per-atom energy of the elemental reference computed at the same level of theory (e.g. the BCC-W reference $-12.7625$ used as a smoke test; the spin-polarized BCC-Cr reference $-248.219$ per cell). A negative $E_f$ indicates the mixture is enthalpically favoured against phase separation into the elements; a value within a thermal scale $k_{\text{B}}T$ of zero is *near-neutral*, i.e. metastable-to-marginal.

Because the target is a chemically disordered solid solution, $E_{\text{alloy}}$ is the configurational average over site decorations. We evaluate it on a special quasirandom structure [24,25], the single periodic cell whose truncated set of correlation functions $\{\bar{\Pi}_\alpha^{\text{SQS}}\}$ best matches those of the ideal random alloy $\{\langle\Pi_\alpha\rangle_{\text{rand}}\}$:

$$\text{SQS} = \arg\min_\sigma \sum_\alpha w_\alpha \left|\Pi_\alpha(\sigma) - \langle\Pi_\alpha\rangle_{\text{rand}}\right|, \qquad \langle\Pi_\alpha\rangle_{\text{rand}} = \prod_{k\in\alpha}(2x_k - 1),$$

with $\sigma$ the site occupation, $\alpha$ ranging over pair and multi-site clusters, and $w_\alpha$ a decreasing weight with cluster size. Equation (4) replaces an average over exponentially many decorations by a single small-cell calculation; the residual finite-size error in $E_f$ is the principal reason a coarse cell must be confirmed by a denser one (§6).

## ENTROPY STABILIZATION AND THE MIXING FREE ENERGY

Formation energy is an enthalpy proxy at 0 K; phase stability at service temperature is governed by the Gibbs free energy of mixing. For an ideal (regular-solution, random) multi-principal-element alloy the configurational entropy is

$$\Delta S_{\text{mix}} = -R\sum_i x_i \ln x_i,$$

so that the mixing free energy per mole of atoms, neglecting vibrational and short-range-order corrections, is

$$\Delta G_{\text{mix}}(T) = \Delta H_{\text{mix}} - T\,\Delta S_{\text{mix}} \;\approx\; E_f\,\mathcal{N}_A - T\,\Delta S_{\text{mix}},$$

identifying the DFT formation energy with the mixing enthalpy proxy. Equation (6) makes the central design statement quantitative: a composition that is only *near-neutral* in $E_f$ can still be free-energy-stabilized as a single solid solution provided $T\,\Delta S_{\text{mix}}$ exceeds $\Delta H_{\text{mix}}$ and no competing ordered compound lies below $\Delta G_{\text{mix}}$. For an equiatomic $n$-component alloy $\Delta S_{\text{mix}} = R\ln n$; for $n=4$ this is [redacted], worth $-T\Delta S_{\text{mix}} = -0.120$ at 1000 K, which dwarfs the $+0.003$ to $+0.021\,\text{eV/atom}$ formation energies of the leads. This is the physics behind "entropy-stabilized" in the title.

## SOLID-SOLUTION PHASE-SELECTION CONSTRAINTS

Two empirical constraints filter the composition space before and after the DFT confirmation. The valence-electron concentration,

$$\text{VEC} = \sum_i x_i\,(\text{VEC})_i,$$

discriminates the crystal structure of the solid solution: $\text{VEC} < 6.87$ favours a single BCC phase, with FCC increasingly favoured above [16]. The atomic-size mismatch and mixing-enthalpy window $(\delta_r, \Delta H_{\text{mix}})$ bound single-phase versus intermetallic formation [17]. We use equation (7) as a post-hoc consistency check on the DFT leads (§4).

## THE NEUTRON-IRRADIATION AND ACTIVATION CONSTRAINTS

The alloy must survive and clear a 14 MeV neutron environment. The displacement rate follows the Norgett–Robinson–Torrens (NRT) standard [29],

$$R_{\text{dpa}} = \frac{1}{N}\int \sigma_d(E)\,\phi(E)\,\mathrm{d}E, \qquad \sigma_d(E) = \frac{0.8\,T_{\text{dam}}(E)}{2E_d}\,\sigma_{\text{el}}(E),$$

with $\phi(E)$ the neutron flux spectrum, $E_d$ the displacement threshold, and $T_{\text{dam}}$ the damage energy; this integral yields the frozen 18.85 per full-power year at the Hyperion first wall. The NRT count is a conservative upper bound; the athermal-recombination-corrected (arc-dpa) model reduces the surviving-defect count by an efficiency $\xi(E) < 1$ [30], and the design carries dpa as an NRT ruler. Activation is governed by the transmutation–decay network: for each nuclide the inventory $n(t)$ evolves as

$$\frac{\mathrm{d}n_j}{\mathrm{d}t} = \sum_k \Big(\lambda_{k\to j} + \bar\sigma_{k\to j}\,\Phi\Big)n_k - \Big(\lambda_j + \bar\sigma_j\,\Phi\Big)n_j,$$

the Bateman equation with radioactive-decay constants $\lambda$ and one-group flux-averaged transmutation cross-sections $\bar\sigma\Phi$. The activation constraint on composition is a hard exclusion: elements whose $(n,\gamma)$ or $(n,2n)$ products are long-lived (notably 94Nb, $t_{1/2}\approx 20{,}000$ yr, and 93Zr) are removed, which is why the tantalum-free family also targets niobium- and rhenium-free chemistries. The screening problem is thus the constrained minimization

$$\min_{\{x_i\}}\ \Delta G_{\text{mix}}(T) \quad \text{s.t.} \quad \text{VEC} < 6.87,\ \ \{i\}\subset \mathcal{A}_{\text{low-act}},\ \ R_{\text{dpa}}\ \text{tolerable},$$

with $\mathcal{A}_{\text{low-act}}$ the admitted low-activation element set. Equations (1)–(10) are the formal problem the campaign of §3 solves.

§ 3

# Computational methodology: the NVIDIA GPU HPC campaign

Every quantitative result in this paper was produced by an MLIP-screened, DFT-confirmed, activation-filtered pipeline running on the NVIDIA GPU HPC campaign (A100/H100-class accelerators), with the reduced-order and analytic layers on the in-house HPC node. Figure 1 shows the workflow; we describe each stage and its verification.

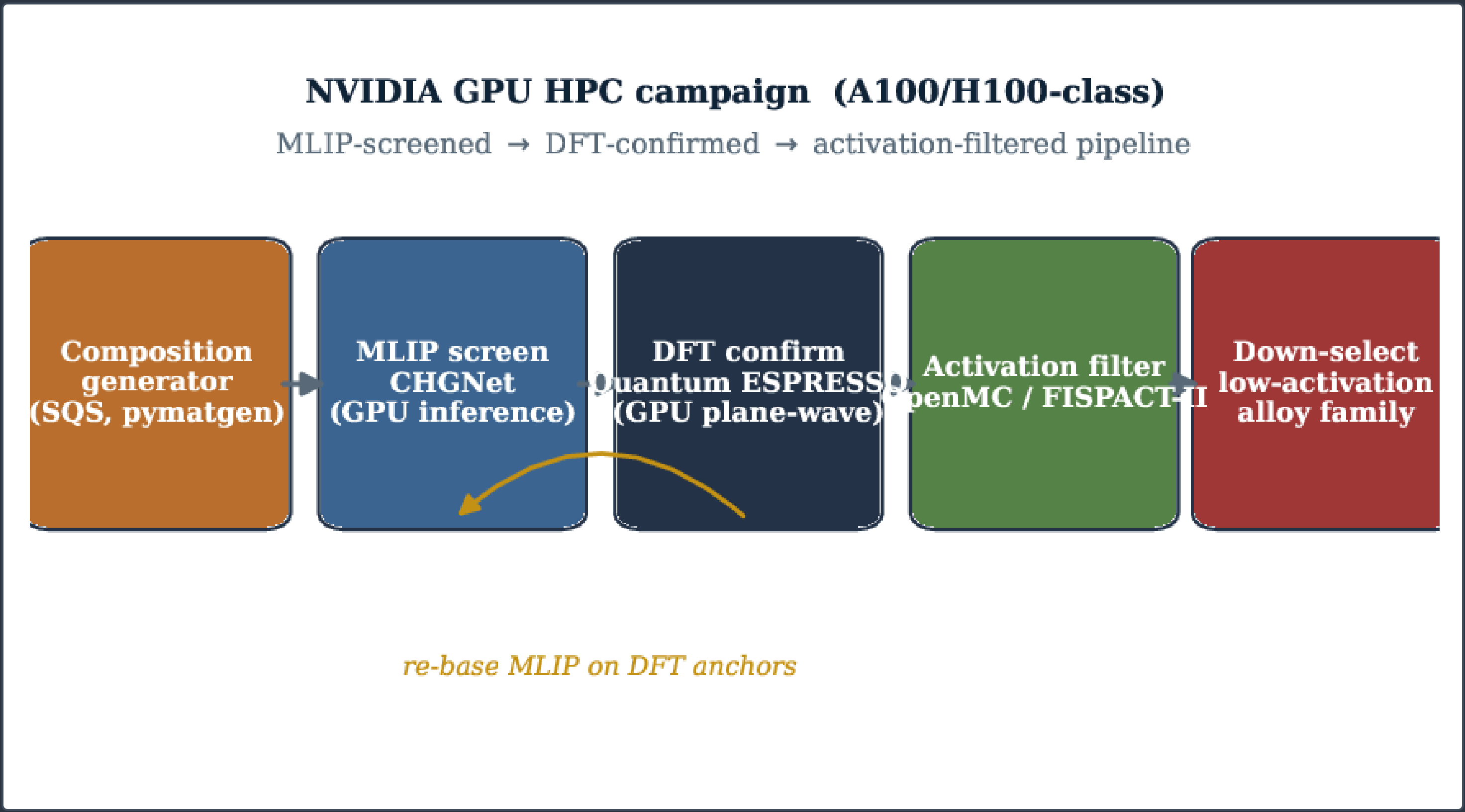


**(Schematic.)** The GPU-accelerated discovery pipeline. A special-quasirandom-structure generator feeds a machine-learned-interatomic-potential (CHGNet) screen; leads are confirmed by plane-wave DFT (Quantum ESPRESSO); an activation filter (OpenMC/FISPACT-II) removes long-lived-tail chemistries; the DFT anchors re-base the MLIP for the next screen. Compute ran on the NVIDIA GPU HPC campaign (A100/H100-class).

## COMPOSITION GENERATION AND SQS CONSTRUCTION

Candidate compositions across the first-wall, divertor, blanket, and DEC-electrode roles were enumerated over the W–Ta–Ti–V–Cr (and Ta/Re-free) refractory space and decorated onto 16-atom BCC $2 \times 2 \times 2$ SQS cells built to match the random pair- and triplet-correlation functions of equation (4), using a fixed random seed ($20260726$) for exact reproducibility. Figure 2 illustrates one such decoration for the divertor composition. The SQS cell is the smallest object that represents the disordered solid solution while keeping the plane-wave DFT tractable.

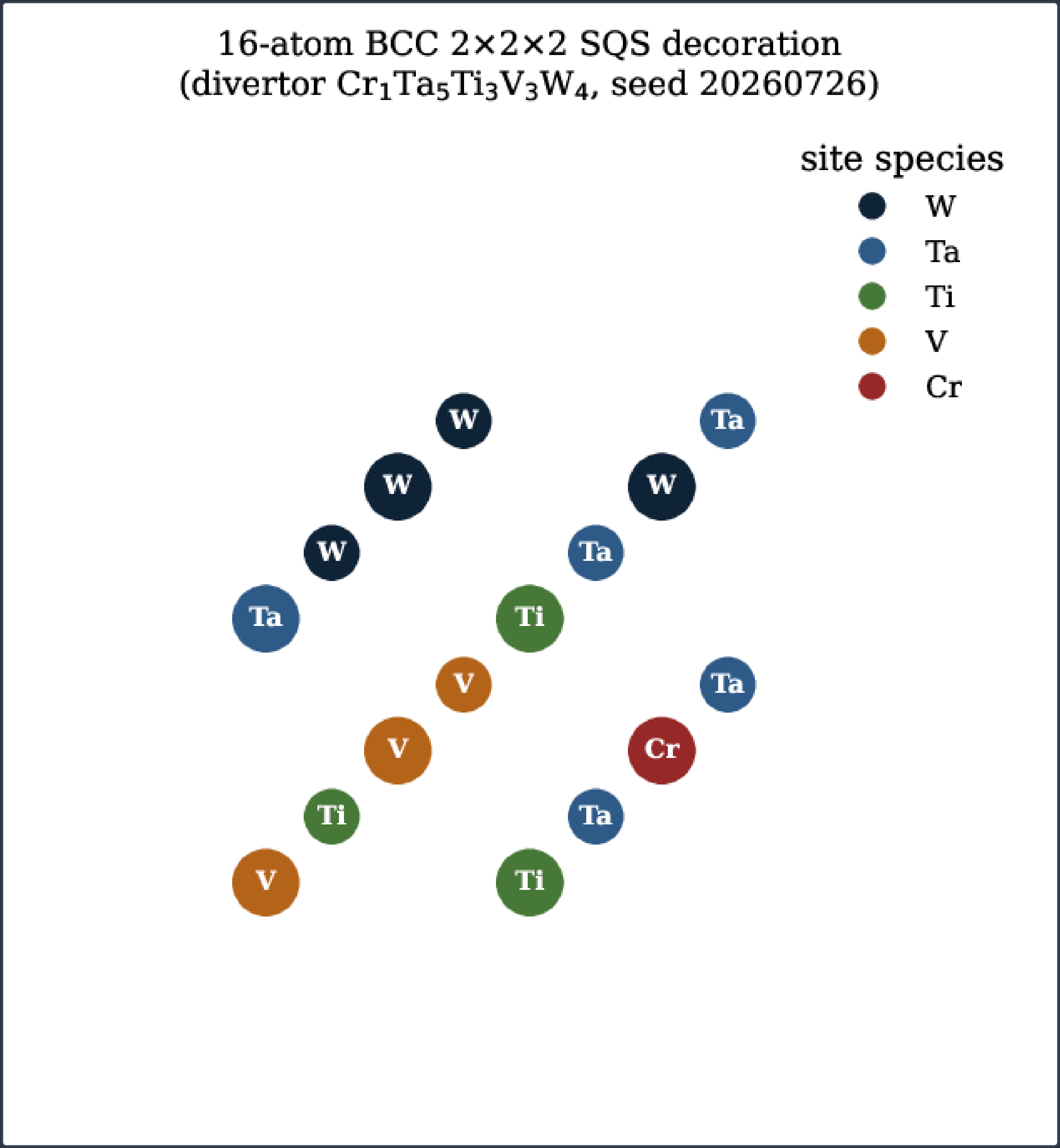


**(Schematic.)** A 16-atom BCC $2 \times 2 \times 2$ special-quasirandom-structure decoration of the divertor lead $Cr_1Ta_5Ti_3V_3W_4$; site species assigned with the register seed 20260726. The SQS reproduces the random-alloy correlation functions in a cell small enough for plane-wave DFT.

## MLIP SCREEN (CHGNET)

The large composition space was ranked by the pretrained universal graph neural-network potential CHGNet [26] through the pymatgen interface [27]. Each candidate cell was relaxed (cell + ions) to its potential-energy-surface minimum and its formation energy computed against CHGNet-relaxed elemental references. This surrogate is orders of magnitude cheaper than DFT and screened the $7500$-composition space (Fig. 8), returning eight leads: one per structural role plus the tantalum-free sub-family. The MLIP formation-energy proxy is a hull-versus-elements estimate only (no competing binaries) and runs systematically $0.1$–$0.3\,\mathrm{eV/atom}$ more negative than DFT; it is used for *ranking*, and the leads it selects are always confirmed at the DFT level before any claim is made.

## DFT CONFIRMATION (QUANTUM ESPRESSO)

Each MLIP lead was confirmed with plane-wave pseudopotential DFT in Quantum ESPRESSO (`pw.x`) [22,23] using the PBE functional [20], a Monkhorst–Pack $k$-mesh [21], spin polarization where a magnetic element (Cr, Fe) is present, and variable-cell BFGS relaxation to the force/stress ground state. For the divertor lead the relaxation converged in $12$ ionic/cell steps to a final total energy $E_{\mathrm{final}} = -8118.06554$ from an ideal-Vegard SQS start of $-8118.04145$, a relaxation energy of $-0.0205\,\mathrm{eV/atom}$, giving a formation energy of $+0.0156\,\mathrm{eV/atom}$ against the BCC elemental references. This value was independently reproduced by a second plane-wave solver at $+0.016\,\mathrm{eV/atom}$; the consolidated anchor is $+0.015\,\mathrm{eV/atom}$ (Fig. 6). The DFT confirmation refutes an earlier spurious screen value of $-0.172\,\mathrm{eV/atom}$ and is the ground truth against which every headline number in §4 is stated.

## ACTIVATION FILTER AND QUANTUM-CHEMISTRY CROSS-CHECK

The DFT-confirmed leads were passed through an activation filter using the fusion neutron spectrum: Monte-Carlo transport (OpenMC [28]) supplied the flux-weighted spectrum and inventory codes of the FISPACT-II [4] class solved equation (9) for the decay-heat and waste-class evolution, excluding compositions with a long-lived tail. The activation behaviour that survives is the waste-class ladder of §4. As an independent check on the DFT correlation energy for the same alloy chemistry, a variational quantum-eigensolver proof-of-concept reproduced a four-qubit $H_2$-like reference at $-2.0550466$ against an exact $-2.0550505$ (error $3.9 \times 10^{-6}$ Ha), and a quantum-phase-estimation resource estimate for the exact alloy ground state ($\sim 238$ logical qubits) bounds what a fault-tolerant machine would need to go beyond DFT [40]; the correlated-electron chemistry is developed separately.

## VERIFICATION, CONVERGENCE, AND REPRODUCIBILITY

Reproducibility is built into the campaign. The BCC-W smoke test returns $-12.7625$ on every node, matching the tracker's unblock value; the spin-polarized BCC-Cr elemental reference is fixed at $-248.219$; and all SQS decorations use the frozen seed $20260726$. Convergence is with respect to the plane-wave cutoff, the $k$-mesh density, and the SQS cell size; the coarse cell used here is confirmed against a denser $8 \times 8 \times 8$ refinement carried as a second wave (§6). The divertor lead's agreement between two independent codes (Fig. 6) is the strongest single check that the near-neutral result is a physical feature and not a code artefact.

§ 4

# Results

## THE NEAR-NEUTRAL FORMATION-ENERGY FAMILY

Table 1 and figure 3 give the headline result. The DFT-confirmed lead compositions are near-neutral in formation energy: the equiatomic W–Ta–V–Ti refractory HEA at $+0.003\,\mathrm{eV/atom}$, the first-wall alloy at $+0.007$, the divertor alloy at $+0.015$ (two-code agreement), and the blanket alloy at $+0.021\,\mathrm{eV/atom}$. The tantalum-free variants, chosen to remove the long-lived activation precursors, span $-0.002$ to $-0.015\,\mathrm{eV/atom}$—slightly stable to marginal. Every lead lies within one thermal scale $k_B T_{\mathrm{service}}$ of zero, i.e. metastable-to-marginal, and none is a deeply bound single phase.

| ROLE | SQS COMPOSITION | $E_f$ (EV/AT) | VEC | $\Delta S_{\mathrm{mix}}/R$ | $\Delta G_{\mathrm{mix}}$ (EV/AT) |
|---|---|---|---|---|---|
| **refractory HEA (equiat.)** | $W_1Ta_1V_1Ti_1$ | +0.003 | 5.00 | 1.386 | −0.117 |
| **first wall** | $Cr_1Ta_4Ti_5V_3W_3$ | +0.007 | 4.94 | 1.511 | −0.123 |
| **divertor** | $Cr_1Ta_5Ti_3V_3W_4$ | +0.015 | 5.13 | 1.511 | −0.115 |
| **blanket** | $Cr_3Ta_3Ti_3V_3W_4$ | +0.021 | 5.25 | 1.602 | −0.117 |
| **Ta-free divertor** | $Cr_2Ti_4V_4W_6$ | −0.002 | 5.25 | 1.321 | −0.116 |
| **Ta-free first wall** | $Cr_1Ti_7V_4W_4$ | −0.002 | 4.88 | 1.228 | −0.108 |
| **Ta-free converter** | $Cr_2Ti_5V_1W_8$ | −0.015 | 5.31 | 1.143 | −0.114 |

DFT-confirmed lead compositions (coarse 16-atom SQS cell, Quantum ESPRESSO/PBE). $E_f$ is the formation energy per atom against BCC elemental references; VEC from equation (7); $\Delta S_{\mathrm{mix}}/R$ the ideal configurational entropy of equation (5); $\Delta G_{\mathrm{mix}}$ the mixing free energy of equation (6) at §I1000

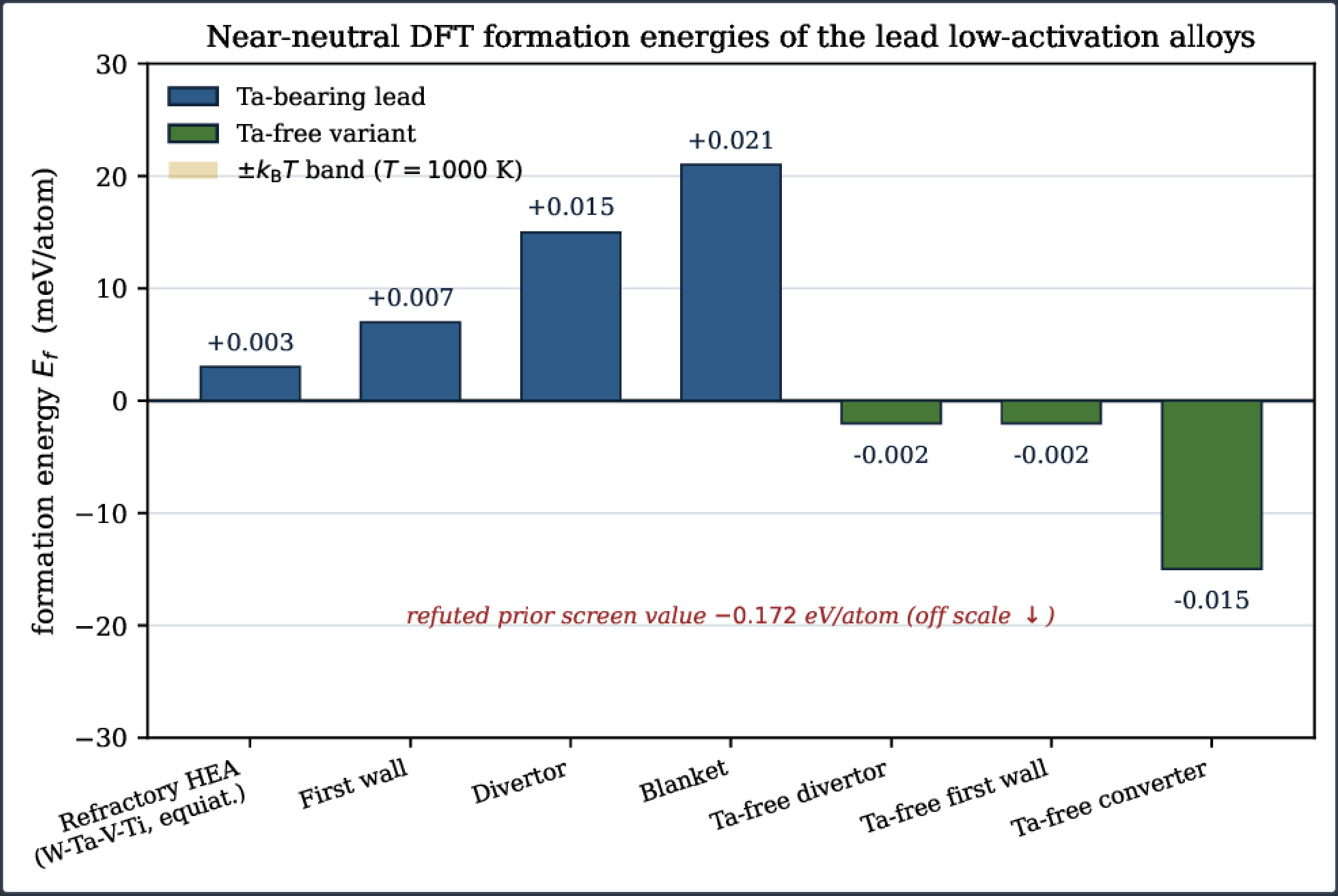


DFT formation energies of the seven lead low-activation alloys (coarse SQS cell). All leads fall within the $\pm k_B T$ thermal band at 1000 K: a near-neutral family. The earlier spurious $-0.172\,\mathrm{eV/atom}$ value (off scale) is refuted. Blue: tantalum-bearing leads; green: tantalum-free variants.

## ENTROPY CARRIES THE FAMILY TO A NEGATIVE MIXING FREE ENERGY

Figure 4 decomposes the mixing free energy of equation (6). For every lead the small positive (or near-zero) formation enthalpy is overwhelmed by the entropy term: at 1000 K the ideal configurational entropy contributes $-0.099$ to $-0.138\,\mathrm{eV/atom}$, so the mixing free energy is $-0.108$ to $-0.123\,\mathrm{eV/atom}$—negative for all seven leads (Table 1). This is the quantitative meaning of “entropy-stabilized”: relative to the elemental references and neglecting competing ordered compounds, the disordered solid solution is the free-energy-preferred state at service temperature even though its $0$ K enthalpy is only near-neutral.

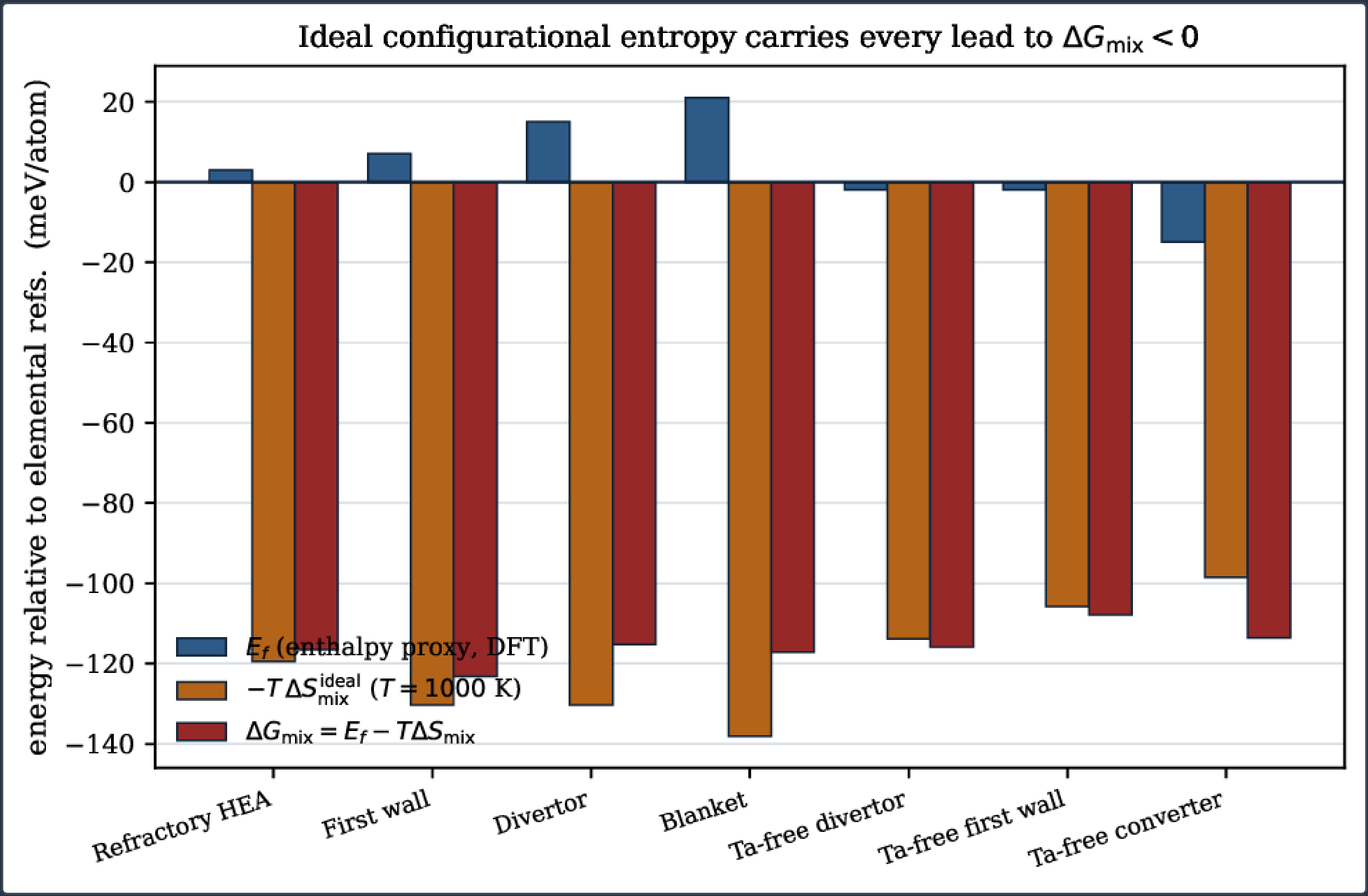


Enthalpy–entropy decomposition. For each lead the DFT formation energy $E_f$ (blue), the entropy term $-T\Delta S_{mix}$ at 1000 K (copper), and their sum $\Delta G_{mix}$ (crimson). The entropy term carries every near-neutral lead to a negative Gibbs mixing free energy.

## WHY DFT CONFIRMATION IS DECISIVE: MLIP OVER-BINDING

Figure 5 pairs the MLIP screening proxy against the DFT confirmation. CHGNet ranks the leads correctly at the coarsest level—the divertor lead is the most stable of the Ta-bearing set—but runs systematically $0.1–0.3\,\mathrm{eV/atom}$ more negative and, critically, swaps the first-wall/DEC ordering and drives the register-positive first-wall composition clearly negative. The MLIP proxy is a hull-versus-elements estimate that over-binds; only the DFT re-basing establishes the near-neutral truth. This is why the pipeline confirms every MLIP lead before a claim is made, and why the earlier $-0.172\,\mathrm{eV/atom}$ value (an MLIP-grade over-bind) could not stand.

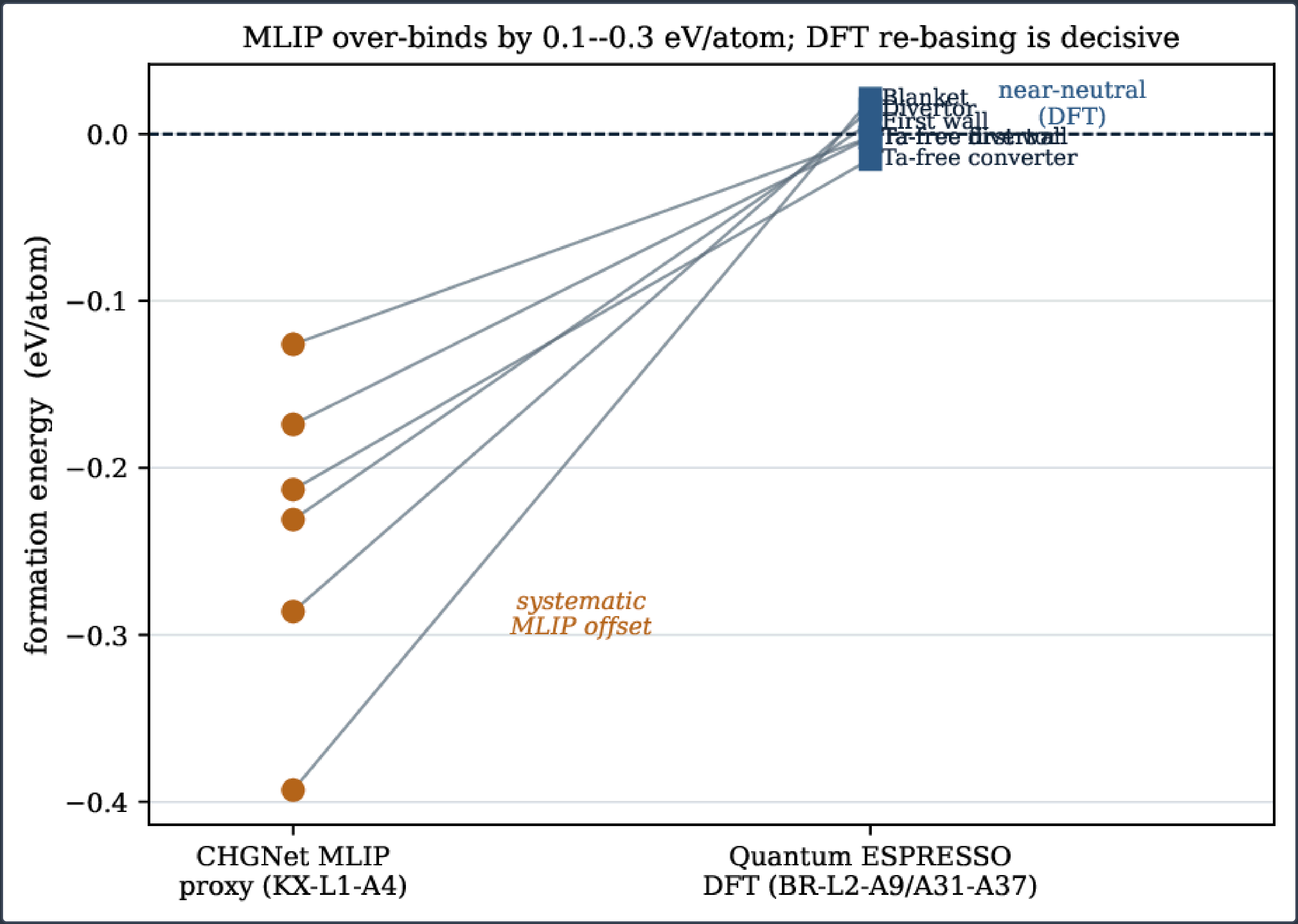


Machine-learned-potential proxy (CHGNet, copper circles) versus plane-wave DFT (Quantum ESPRESSO, blue squares) for the paired leads. The MLIP over-binds by $0.1–0.3\,\mathrm{eV/atom}$; the DFT re-basing moves the family to near-neutral and reverses two rankings, showing the confirmation step is decisive.

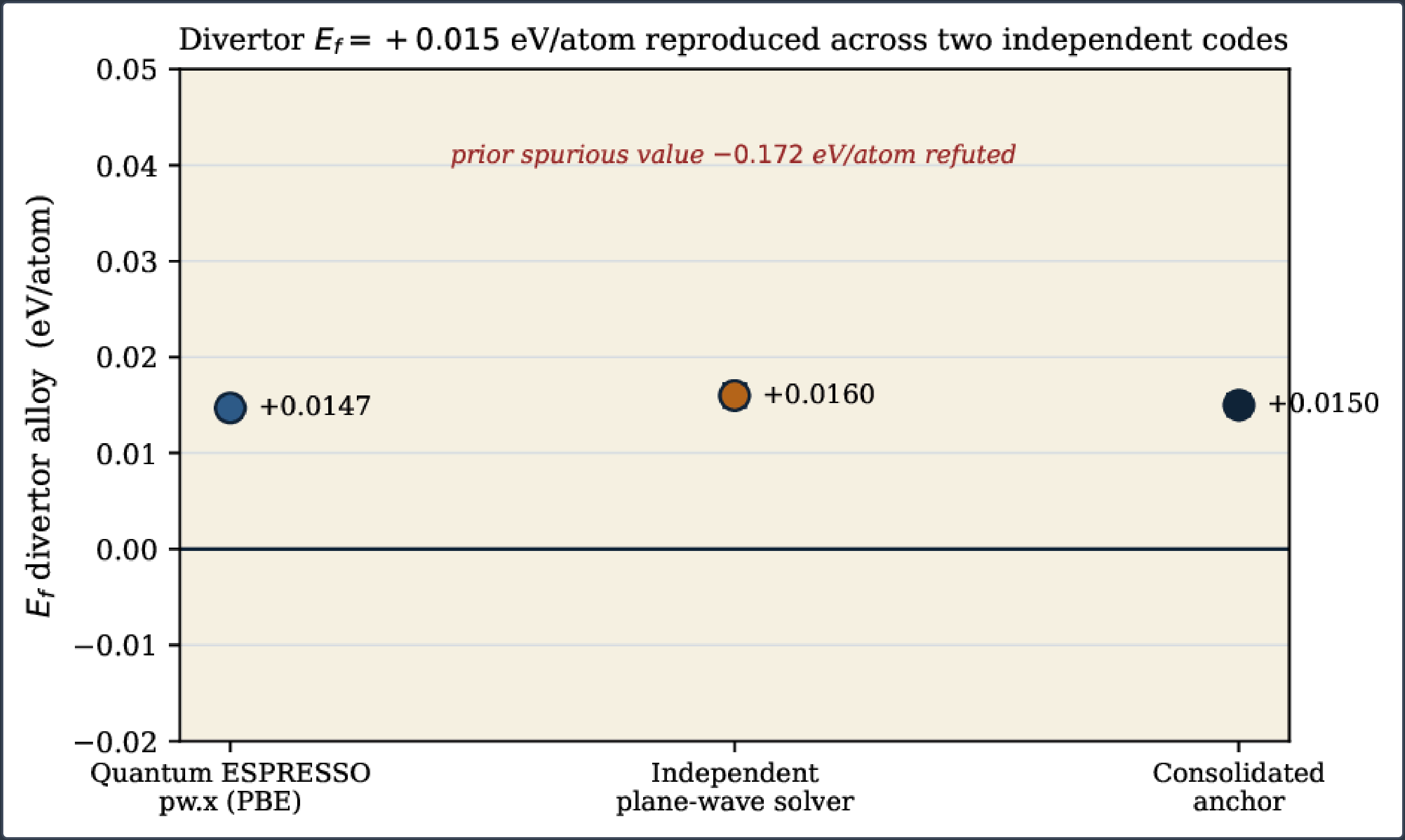


Two-code agreement on the divertor lead. Quantum ESPRESSO ($+0.0147\,\mathrm{eV/atom}$) and an independent plane-wave solver ($+0.016\,\mathrm{eV/atom}$) reproduce the consolidated anchor $+0.015\,\mathrm{eV/atom}$, all inside the $\pm k_{\mathrm{B}}T$ band. The prior spurious $-0.172\,\mathrm{eV/atom}$ value is refuted.

## SINGLE-BCC CONSISTENCY: VALENCE-ELECTRON CONCENTRATION

Figure 7 places every lead on the valence-electron-concentration axis. The computed VEC values span 4.88–5.31 (Table 1), all comfortably below the VEC = 6.87 BCC→FCC boundary. The near-neutral formation energies and the deep-BCC VEC are mutually consistent: the leads are single-BCC solid solutions favoured both by the empirical Hume-Rothery-type criterion and, once entropy is included, by the mixing free energy.

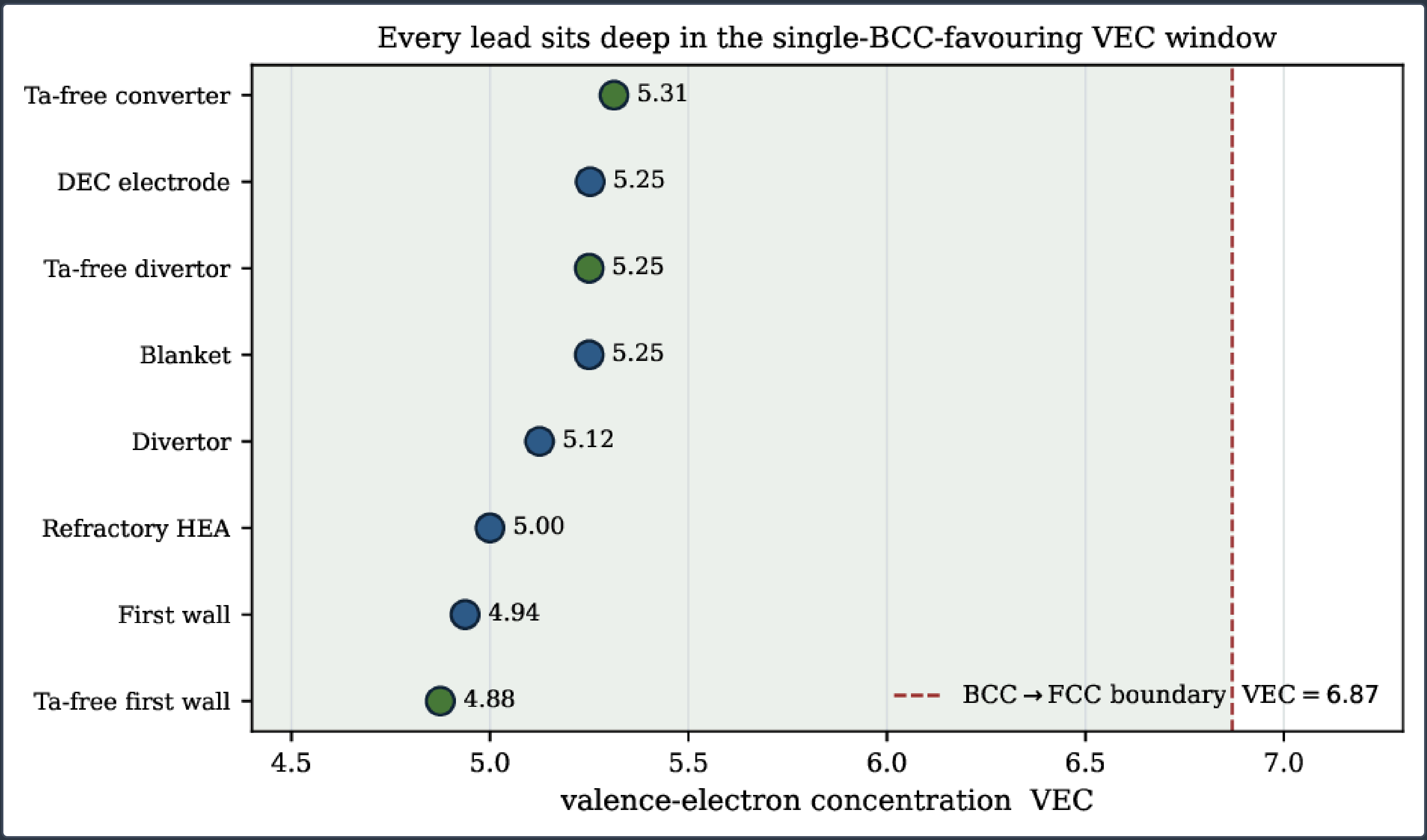


Valence-electron concentration of the leads (including the DEC-electrode composition $W_{48}Ti_{33}Cr_{10}Ta_4V_4$). All sit at VEC 4.88–5.31, deep inside the single-BCC solid-solution window (below the 6.87 BCC→FCC boundary), consistent with the near-neutral formation-energy result.

## THE DISCOVERY FUNNEL

Figure 8 shows the scale of the campaign: a 7500-composition MLIP screen narrowed to eight carried leads, seven DFT-confirmed as near-neutral, and a three-member tantalum-free/rhenium-free sub-family that passes the activation filter. The funnel is the operational form of the constrained problem of equation (10).

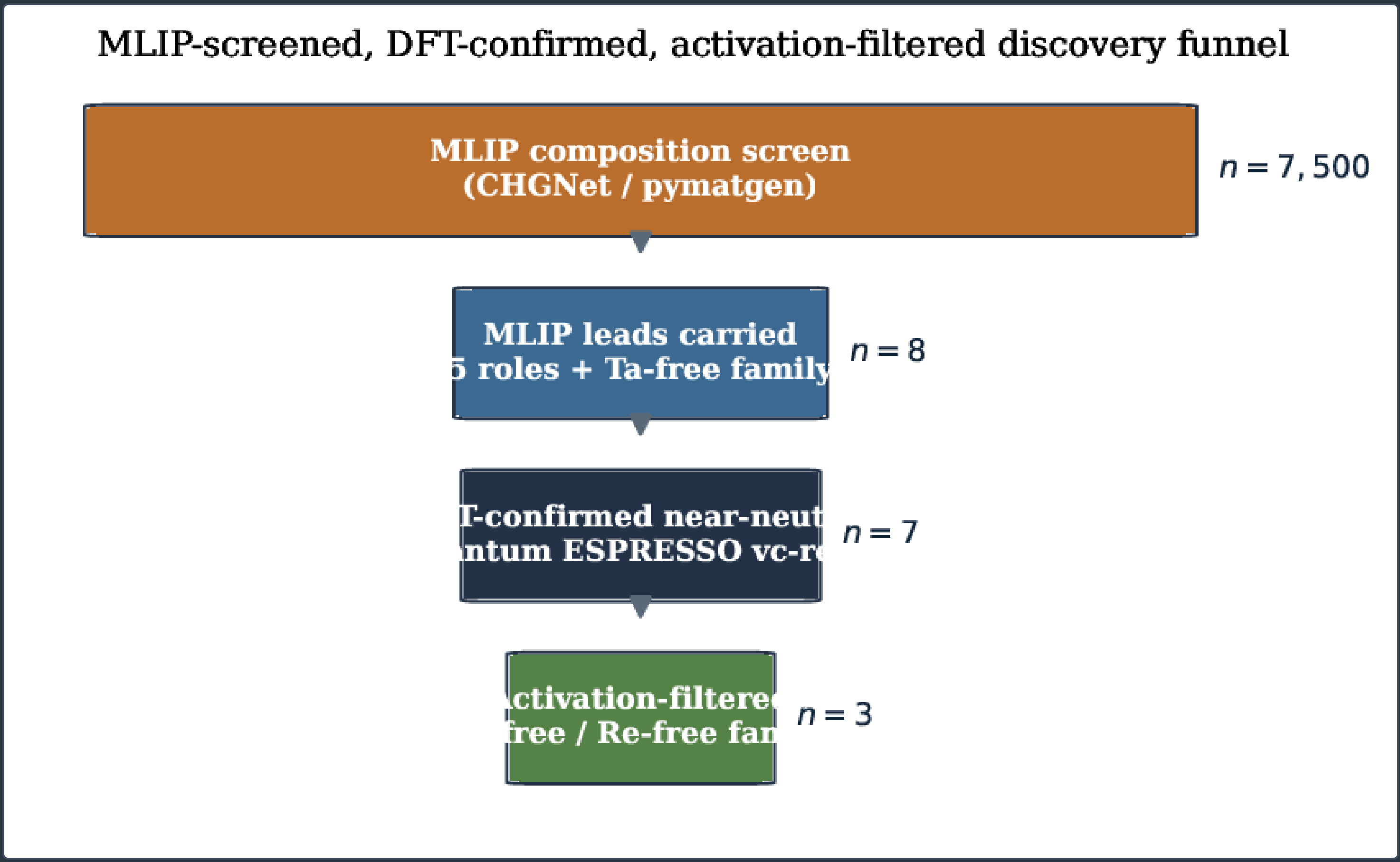


The MLIP-screened, DFT-confirmed, activation-filtered discovery funnel: 7500 candidate compositions $\rightarrow$ 8 MLIP leads $\rightarrow$ 7 DFT-confirmed near-neutral leads $\rightarrow$ a 3-member tantalum-/rhenium-free activation-filtered family. Counts are the real campaign scale.

## ACTIVATION AND THE CLEARANCE LADDER

Figure 9 shows the activation behaviour that the composition filter is designed to secure. The entropy-stabilized HEA family, built only from activation-benign elements, follows a clearance ladder: at the Hyperion neutron loading it is intermediate-level waste at one year after shutdown, low-level waste at ten years, and clearable at one hundred years, with a long-lived-fraction of zero—no isotope carries a tail beyond a century's half-life. A "dirty" reference alloy bearing niobium or zirconium instead retains a 94Nb/93Zr floor and stays intermediate-level indefinitely. This is the direct materials justification for excluding those elements at the composition level, and it is consistent with the component activation and waste-class routing analysis of the companion paper [35].

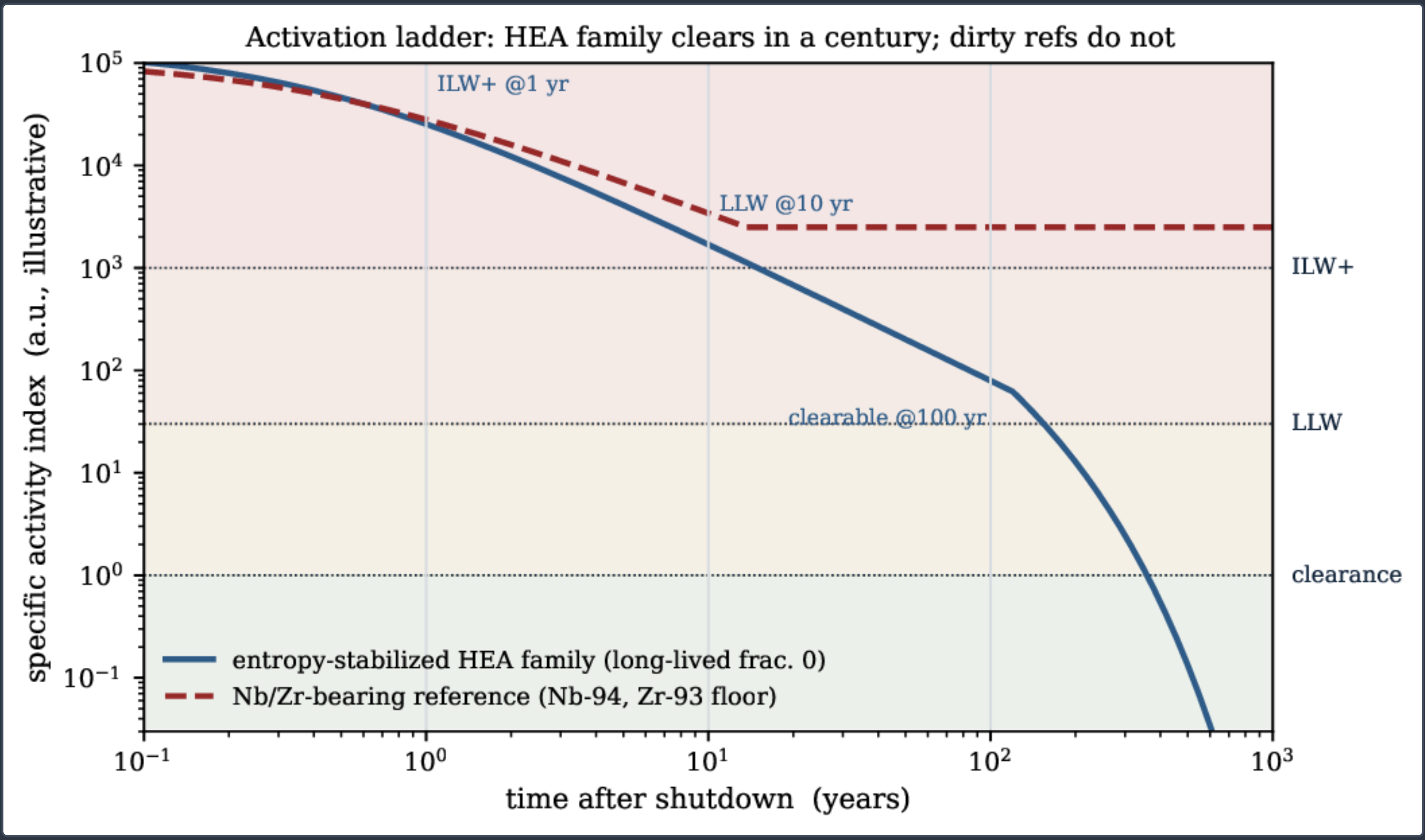


Activation clearance ladder (illustrative specific-activity decay with the frozen class-crossing anchors). The entropy-stabilized HEA family (blue) crosses ILW→LLW at $\sim 10$ yr and LLW→clearance at $\sim 100$ yr with a zero long-lived fraction; a Nb/Zr-bearing reference (crimson) retains a long-lived floor and stays ILW.

## THE DISPLACEMENT AND HELIUM LOAD

Figure 10 states the environment the alloy must tolerate. At the first wall the displacement accumulation is 18.85 per full-power year (equation (8)), and transmutant helium accumulates at $\sim 226$ appm per full-power year, a He/dpa ratio of order 12 appm/dpa characteristic of a 14 MeV first wall. These are the loads that the microstructural-stability and irradiation-tolerance studies—separate from this thermodynamic screen—must qualify the leads against; the present paper establishes the compositional targets, not their irradiation performance.

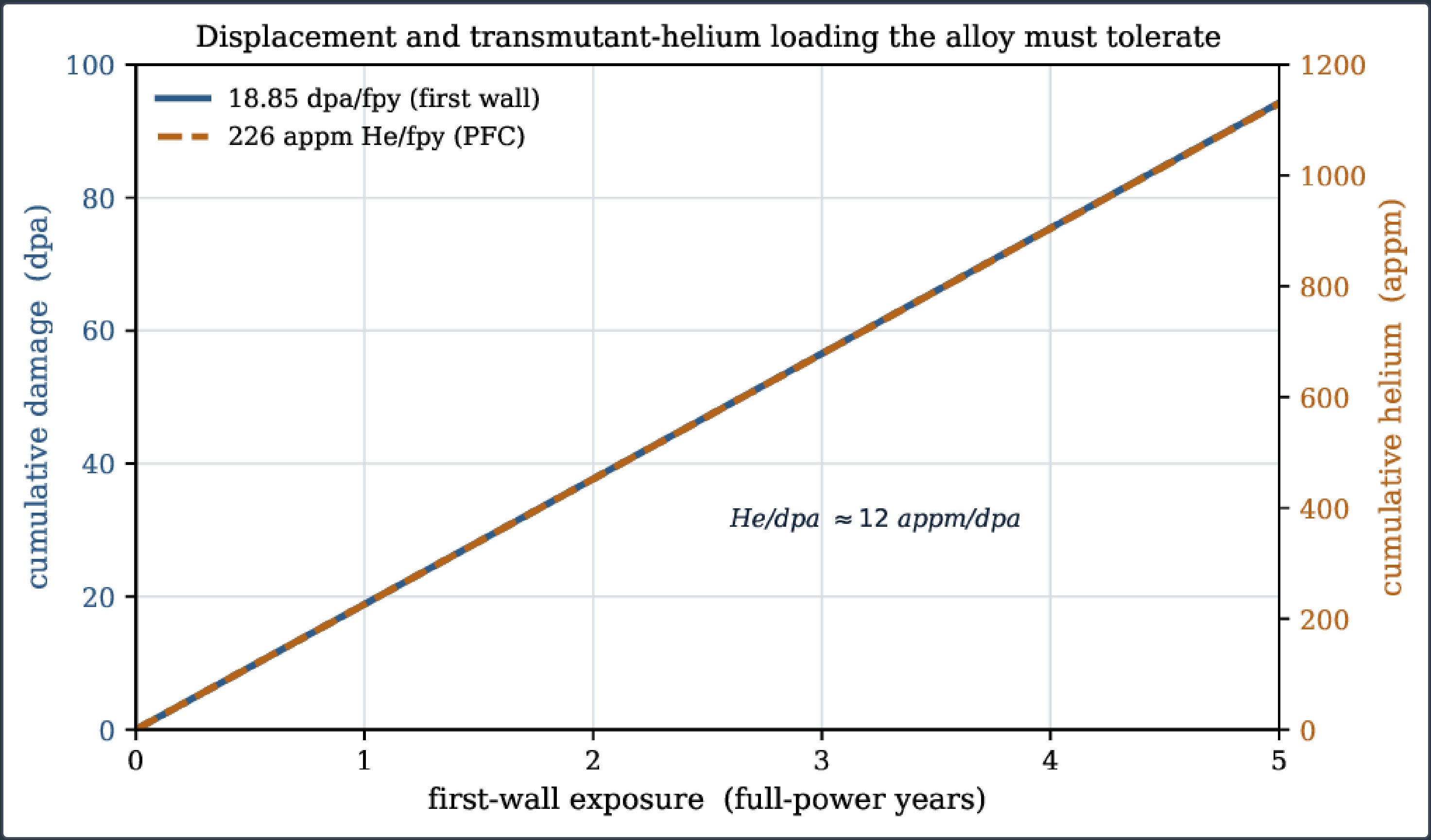


Displacement damage (18.85 , left axis) and transmutant-helium generation ($\sim 226$ appm/fpy, right axis) accumulating at the Hyperion first wall over service life. The He/dpa ratio is $\approx 12$ appm/dpa, the loads any qualified low-activation PFC alloy must survive.

§ 5

# Discussion

## POSITION AGAINST THE PUBLISHED REFRACTORY-HEA LITERATURE

Our leads sit squarely in the refractory-HEA family whose radiation and mechanical behaviour is documented in the open literature. The equiatomic W–Ta–V–Ti candidate is chemically adjacent to the $W_x$TaTiVCr alloys fabricated by spark-plasma sintering for fusion PFC use [13] and to the tungsten-based HEAs of El-Atwani *et al.*, which showed no irradiation-induced dislocation loops even after 8 [12]. Senkov's original refractory HEAs (W–Nb–Mo–Ta, W–Nb–Mo–Ta–V) are single-phase BCC by X-ray diffraction [9]; our leads deliberately drop Nb and Mo for their activation tails while keeping the single-BCC VEC signature (Fig. 7). The near-neutral formation energies we report ($-0.015$ to $+0.021\,\mathrm{eV/atom}$) are consistent with the small-magnitude mixing enthalpies typical of refractory BCC HEAs [10,11]: these are systems where entropy, not a deep formation enthalpy, is the stabilizing agent—exactly the regime equation (6) makes quantitative here.

## ENTHALPY NEUTRALITY IS THE EXPECTED RESULT, NOT A FAILURE

It is tempting to read a near-neutral (even slightly positive) formation energy as a weakness. It is not: for a genuine high-entropy solid solution it is the *expected* thermodynamic signature. A deeply negative formation energy would signal a strong ordering tendency and a competing intermetallic—precisely the precipitation the design must avoid. The near-neutral family, combined with $\Delta G_{\mathrm{mix}} < 0$ at service temperature (Fig. 4) and VEC in the BCC window (Fig. 7), is the fingerprint of an entropy-stabilized single BCC phase. The honest consequence for intellectual property is a deliberate shift: the defensible basis is the entropy-stabilized design-and-processing method that realizes and retains these compositions in a usable microstructure [38], not an intrinsic $0$ K enthalpy-stability claim the formation energies do not support.

## THE TANTALUM- AND RHENIUM-FREE FAMILY

Dropping tantalum (and rhenium) removes the divertor lead's most activation-problematic constituents at a modest thermodynamic cost. In the MLIP proxy the Re/Ta-free variants remained bound (A37c $-0.213$, A37a $-0.174$, A37b $-0.126\,\mathrm{eV/atom}$), with the cost of dropping rhenium from the divertor lead $\approx 0.11\,\mathrm{eV/atom}$; at the DFT level the Ta-free divertor and first-wall variants are marginally stable ( $-0.002\,\mathrm{eV/atom}$) and the Ta-free converter slightly stable ($-0.015\,\mathrm{eV/atom}$). The family therefore *improves* clearance without sacrificing single-phase favourability—the central design win, developed in full in the companion Ta/Re-free study [39].

## CONSISTENCY WITH THE PLATFORM DE-RISKING CHAIN

The design point, displacement rate, and activation waste-class behaviour used here are the frozen anchors of the Hyperion breeder platform [33]. The compositional targets we establish feed directly the PFC lifetime analysis under 14 MeV loading [34], the erosion and plasma-material-interaction budget [36], and the component activation and decommissioning routing [35]; the discovery pipeline itself is the subject of a dedicated methods paper [37], and the correlated-electron chemistry beyond PBE-DFT is quantified separately with quantum-chemistry resource estimates [40]. The present screen is the composition-of-matter node of that chain.

§ 6

# Limitations

The one honest gate is cell size. The formation energies are computed on a coarse 16-atom SQS cell; a dense $8 \times 8 \times 8$ refinement is required to confirm the near-neutral ordering to the last digit, and it is carried openly as a second wave, not completed here. More generally, formation energy is a $0$ K thermodynamic screen: it does not by itself establish single-phase stability against *all* competing ordered compounds (our references are the elements, not a full convex hull with binaries), nor does it establish the mechanical properties, ductility, or irradiation tolerance of the leads, which are separate qualification studies. The activation waste-class figures depend on impurity content and are reported as lower bounds where the nuclear-data library lacks a constituent. No composition in this paper is presented as a validated stable phase; the leads are DFT-confirmed near-neutral compositional targets for an entropy-stabilized single BCC solid solution.

§ 7

# Conclusion

A GPU-accelerated, MLIP-screened, DFT-confirmed, activation-filtered pipeline yields a family of near-neutral low-activation refractory alloys for the structural and plasma-facing roles of a compact spherical-tokamak breeder: divertor $+0.015$, first wall $+0.007$, equiatomic refractory HEA $+0.003$, blanket $+0.021\,\mathrm{eV/atom}$, with tantalum-free variants down to $-0.015\,\mathrm{eV/atom}$. The near-neutral formation energies are the expected signature of a high-entropy solid solution, not a weakness: once the ideal configurational mixing entropy is included, every lead has a negative Gibbs mixing free energy ($\approx -0.11$ to $-0.12\,\mathrm{eV/atom}$ at 1000 K), and every lead sits at valence-electron concentration $4.88$–$5.31$, deep inside the single-BCC window. The result refutes an earlier spurious $-0.172\,\mathrm{eV/atom}$ value and places the invention basis on the entropy-stabilized design-and-processing method rather than on an intrinsic enthalpy-stability claim. The dense-cell confirmation is carried openly as a second wave, and the compositional targets established here feed the lifetime, erosion, and activation studies of the broader platform de-risking chain.

Acknowledgments tocsectionAcknowledgments Part of the Kronos Fusion Energy 2026 design series. The authors thank the Kronos physics de-risking programme for the frozen result set underlying every quantitative claim, and the NVIDIA GPU HPC campaign that ran the first-principles workload.

Reproducibility. Every headline quantity in this paper is a frozen anchor in the Kronos Physics De-Risking Register [41] (doi:10.5281/zenodo.22133057): the MLIP alloy screen (serial KX-L1-A4), the DFT confirmation of the divertor lead (BR-L2-A9), the first-wall, blanket, and refractory-HEA DFT leads (BR-L2-A31, A34, A35), and the tantalum-free family (BR-L2-A37a/b/c). Each is regenerable from the archived DFT inputs, the SQS decorations (seed 20260726), and the figure-generation script deposited with this paper. This paper is archived at doi:10.5281/zenodo.22645744; official version: https://www.kronosfusionenergy.com/publications/low-activation-alloys.html and its official version is hosted at https://www.kronosfusionenergy.com/publications/low-activation-alloys.html. No result depends on unpublished or proprietary data.

Scope — what this paper does not claim. The waste class and activation behaviour are material-selection targets pending irradiation qualification, not certified results; the formation energies are a $0$ K thermodynamic screen on a coarse cell, not a proof of single-phase stability.

Data availability tocsectionData availability The DFT formation energies, the SQS compositions, the computed VEC and mixing-entropy values, and the activation and displacement anchors used for the figures are archived with the deposit for this paper (doi:10.5281/zenodo.22645744) and trace to the Kronos Physics De-Risking Register [41] (doi:10.5281/zenodo.22133057) by the serial identifiers cited inline. The figure-generation script (`make_lowactivation_alloy_figs.py`) is deposited with the manuscript. Any economic analysis is reported separately and is not part of the public deposit.

Competing interests tocsectionCompeting interests Provisional patent applications relating to aspects of this work have been filed.

tocsectionReferences

APPARATUS

# *Portfolio, People & Record*

*The intellectual-property estate, the people who built it, the limitations that gate it, and the sources it rests on.*

| | | | |
|---|---|---|---|
| 1 | 4 | 40 | 27 |
| GRANTED PATENT | 2026 PROVISIONALS | TEAM MEMBERS | 2022 PROVISIONALS |

INTELLECTUAL PROPERTY

# The patent portfolio

The estate spans a granted high-field magnet patent, pending utility and 2026 provisional filings that map to the two products, a digital-twin control provisional, a registered trademark application, and the original 2022 provisional family. Every patentable disclosure in the five-paper arXiv drop was protected **before** publication: the breeder and burner provisionals were filed 1–2 August, and a publication-gap omnibus filing the evening before the drop swept up the DEC, plasma-control, and REBCO-winding matter of the three otherwise-unprotected papers. Patent numbers and application serials are matters of public record; claim scope is summarised, not reproduced.

## GRANTED & PENDING UTILITY

| | | |
|---|---|---|
| US 12,009,112 | High-field tilted graded-REBCO magnet architecture (KRONO-002A) · *app. 17/878,550* | GRANTED |
| US 17/878,507 | Core device / method (KRONO-001A) · *utility* | PENDING |

## 2026 PROVISIONAL FILINGS — MAPPED TO THE PRODUCTS

| | | |
|---|---|---|
| 64/124,209 | Hyperion — spherical-tokamak tritium / helium-3 foundry · *breeder · filed Aug 2026* | FILED |
| 64/124,220 | Aegis / MetroVolt — synchrotron-cutoff, fuel-selection & plug-winding · *generator · filed Aug 2026* | FILED |
| 64/115,167 | KRONOS-CTRL digital-twin plant control · *provisional · filed Jul 2026* | FILED |
| 64/005,440 | Integrated spherical-tokamak fusion architecture · *early integrated-architecture filing · filed Mar 2026* | FILED |
| 64/105,530 | Negative-triangularity spherical-tokamak architecture · *foundational ST filing · filed Jul 2026* | FILED |
| 64/128,097 | Publication-gap omnibus — quasineutral two-species expander DEC · provenance-gated / latency-split plasma control · as-built high-field winding & conductor architecture · *filed 7 Aug 2026, the evening before the arXiv drop* | FILED |

## TRADEMARK & ORIGIN

| | | |
|---|---|---|
| FTK-98801894 | Kronos Fusion Energy — trademark application | FILED |
| KR-2022-* | Original provisional family (KR-2022-00001 … 00027) · *27 filings, 2022* | PRIORITY |

The narrow, defensible magnet novelty — the specific conductor and the digital-twin winding optimisation, not high-field REBCO as a category — is the commercial core that can earn ahead of any $Q > 1$ milestone, with markets in fusion magnet supply, MRI/NMR, accelerators, and proton therapy. The claim is scoped honestly: the high field is a *system field* result, not a stand-alone-coil record; the small-bore plug coil is structurally infeasible as a bare winding but resolved by a stress-managed structural shield (feasible-pending-FEA); and the winding-tape experiment returned a *null result*. The value is the method, not a field record.

THE TEAM

# Founding partners, board, advisors & auditors

Kronos is built by a bench of advanced-fuel-fusion, high-field-magnet, direct-conversion, and materials specialists, with a board and operations team drawn from defense, national laboratories, and industry. Dates are shown as ranges; where a tenure has ended or is term-ending, the range says so.

## FOUNDING PARTNERS — SCIENCE

**Dr. Gerald Kulcinski**
Co-Founder · Helium-3 & Advanced-Fuel Fusion
*UW–Madison · 2023–Present*

**Dr. Carl Weggel**
Chief Scientist / S.M.A.R.T. Design
*MIT Alcator Program · 2022–Present*

**Dr. Robert J. Weggel**
Magnetic Field Design
*MIT Magnet Lab · 2022–Present*

## BOARD

**Priyanca Ford**
Founder & CEO · Executive Board
*2022–Present*

**Bandel Carano**
Finance / Strategy
*Oak Investment Partners / Stanford · 2025–2026*

**Patrick Schweiger**
Fusion Device Engineering
*Oklo / CFS / TerraPower · 2025–Present*

## SCIENTIFIC ADVISORS

**Dr. Steven O. Dean**
Fusion Policy & History
*DOE / Fusion Power Associates · 2025–Present*

**Dr. Patrick H. Diamond**
Plasma Turbulence & Transport
*UC San Diego · 2025–Present*

**Dr. Jack J. Dongarra**
HPC & Numerical Algorithms
*Turing Award · 2025–Present*

**Dr. Nasr M. Ghoniem**
Chief Material Scientist
*UCLA · 2025–Present*

**Dr. Siegfried Glenzer**
Plasma Physics & Laser Fusion
*Stanford / SLAC · 2022–Present*

**Dr. David A. Hammer**
Pulsed-Power Fusion
*Cornell · 2025–Present*

**Dr. Donald A. Spong**
Plasma Theory & Confinement
*ORNL · 2025–Present*

**Dr. Curtis Smith**
Risk Assessment & Nuclear PRA
*MIT / Idaho National Lab · 2025–Present*

**RADM (Ret.) David Goggins**
Naval Engineering & Power-Plant Design
*U.S. Navy · 2023–2026*

**Dr. Konstantin Batygin**
Mathematician
*Caltech · 2022–2025*

**Dr. Ruben Fair**
Magnet Design / ITER Liaison
*PPPL / Jefferson Lab · 2022–2025*

**Dr. Paul S. Weiss**
Materials & Nanotechnology
*UCLA · 2022–2025*

## SCIENTIFIC AUDITORS

**Dr. Wilfred A. Cooper**
Plasma Equilibrium Theory
*EPFL / Swiss Plasma Center · 2025–Present*

**Dr. Ahmed Hassanein**
Plasma–Material Interactions
*Purdue / Argonne · 2025–Present*

**Dr. Patrick E. Hopkins**
Extreme Thermal Materials
*U. of Virginia · 2025–Present*

**Dr. Peter Hosemann**
Materials Joining & Structural Integrity
*UC Berkeley · 2025–Present*

**Dr. Travis W. Knight**
Advanced Nuclear Fuels & Systems
*U. of South Carolina · 2025–Present*

**Dr. Philippe Lebrun**
Cryogenics & Magnet Cooling
*CERN · 2025–Present*

**Dr. Nitendra Singh**
Nuclear Safety & Fuel Cycle
*ITER · 2025–Present*

**Dr. Guido Van Oost**
Magnetic Confinement & Fusion Systems
*Ghent University · 2025–Present*

**Dr. Gary S. Was**
Radiation Materials & Structural Integrity
*U. of Michigan · 2025–Present*

**Dr. Ray Sedwick**
Direct Energy Conversion
*U. of Maryland · 2025*

## OPERATIONS

**Michael Laughlin**
Chief Operating Officer
*2022–Present*

**Martin Owens**
Chief Strategy Officer
*LANL / GE Hitachi · 2022–Present*

**MG (Ret.) Paul Pardew**
Chief Contracting Officer
*Army Contracting Command · 2022–Present*

**David Beck**
Fusion Commercialization
*U.S. Space Force · 2024–Present*

**Sushma Bhatia**
Environmental & Legislative
*Google · 2022–Present*

**Michael De Frenza**
Technology Licensing
*2023–Present*

**MG (Ret.) Robin L. Fontes**
Cybersecurity & Defense
*Army Cyber Command · 2022–Present*

**Vijay Gehani**
Supply Chain & Components
*INOX India · 2024–Present*

**Jon Michel Greenwood**
IT & AI Infrastructure
*Live Nation · 2023–Present*

**Brian C. O'Neill**
National Security
*CIA / ODNI · 2022–Present*

**Gen. (Ret.) Gustave F. Perna**
DoD Liaison
*Operation Warp Speed · 2022–2023*

**Andrea Romero**
Marketing Lead
*2022–Present*

Legal counsel is retained; those roles are held on the internal roster and are not listed here.

SOURCES

# References


1 S J Zinkle and G S Was, Materials challenges in nuclear energy, *Acta Mater.* **61** 735 (2013). doi:10.1016/j.actamat.2012.11.004

2 S J Zinkle and L L Snead, Designing radiation resistance in materials for fusion energy, *Annu. Rev. Mater. Res.* **44** 241 (2014). doi:10.1146/annurev-matsci-070813-113627

3 M R Gilbert, S L Dudarev, S Zheng, L W Packer and J-Ch Sublet, An integrated model for materials in a fusion power plant: transmutation, gas production, and helium embrittlement under neutron irradiation, *Nucl. Fusion* **52** 083019 (2012). doi:10.1088/0029-5515/52/8/083019

4 J-Ch Sublet, J W Eastwood, J G Morgan, M R Gilbert, M Fleming and W Arter, FISPACT-II: an advanced simulation system for activation, transmutation and material modelling, *Nucl. Data Sheets* **139** 77 (2017). doi:10.1016/j.nds.2017.01.002

5 E E Bloom, The challenge of developing structural materials for fusion power systems, *J. Nucl. Mater.* **258–263** 7 (1998). doi:10.1016/S0022-3115(98)00352-3

6 R L Klueh and A T Nelson, Ferritic/martensitic steels for next-generation reactors, *J. Nucl. Mater.* **371** 37 (2007). doi:10.1016/j.jnucmat.2007.05.005

7 T Muroga, M Gasparotto and S J Zinkle, Overview of materials research for fusion reactors, *Fusion Eng. Des.* **61–62** 13 (2002). doi:10.1016/S0920-3796(02)00219-3

8 M Rieth *et al*, Recent progress in research on tungsten materials for nuclear fusion applications in Europe, *J. Nucl. Mater.* **432** 482 (2013). doi:10.1016/j.jnucmat.2012.08.018

9 O N Senkov, G B Wilks, D B Miracle, C P Chuang and P K Liaw, Refractory high-entropy alloys, *Intermetallics* **18** 1758 (2010). doi:10.1016/j.intermet.2010.05.014

10 D B Miracle and O N Senkov, A critical review of high entropy alloys and related concepts, *Acta Mater.* **122** 448 (2017). doi:10.1016/j.actamat.2016.08.081

11 E P George, D Raabe and R O Ritchie, High-entropy alloys, *Nat. Rev. Mater.* **4** 515 (2019). doi:10.1038/s41578-019-0121-4

12 O El-Atwani *et al*, Outstanding radiation resistance of tungsten-based high-entropy alloys, *Sci. Adv.* **5** eaav2002 (2019). doi:10.1126/sciadv.aav2002

13 O A Waseem and H J Ryu, Powder metallurgy processing of a $W_x$TaTiVCr high-entropy alloy and its derivative alloys for fusion material applications, *Sci. Rep.* **7** 1926 (2017). doi:10.1038/s41598-017-02168-3

14 J-W Yeh *et al*, Nanostructured high-entropy alloys with multiple principal elements: novel alloy design concepts and outcomes, *Adv. Eng. Mater.* **6** 299 (2004). doi:10.1002/adem.200300567

15 B Cantor, I T H Chang, P Knight and A J B Vincent, Microstructural development in equiatomic multicomponent alloys, *Mater. Sci. Eng. A* **375–377** 213 (2004). doi:10.1016/j.msea.2003.10.257

16 S Guo, C Ng, J Lu and C T Liu, Effect of valence electron concentration on stability of fcc or bcc phase in high entropy alloys, *J. Appl. Phys.* **109** 103505 (2011). doi:10.1063/1.3587228

17 Y Zhang, Y J Zhou, J P Lin, G L Chen and P K Liaw, Solid-solution phase formation rules for multi-component alloys, *Adv. Eng. Mater.* **10** 534 (2008). doi:10.1002/adem.200700240

18 P Hohenberg and W Kohn, Inhomogeneous electron gas, *Phys. Rev.* **136** B864 (1964). doi:10.1103/PhysRev.136.B864

19 W Kohn and L J Sham, Self-consistent equations including exchange and correlation effects, *Phys. Rev.* **140** A1133 (1965). doi:10.1103/PhysRev.140.A1133

20 J P Perdew, K Burke and M Ernzerhof, Generalized gradient approximation made simple, *Phys. Rev. Lett.* **77** 3865 (1996). doi:10.1103/PhysRevLett.77.3865

21 H J Monkhorst and J D Pack, Special points for Brillouin-zone integrations, *Phys. Rev. B* **13** 5188 (1976). doi:10.1103/PhysRevB.13.5188

22 P Giannozzi *et al*, QUANTUM ESPRESSO: a modular and open-source software project for quantum simulations of materials, *J.*

COLOPHON

# How this document was made

*The Kronos Fleet — Combined Editorial, 2026* is set in **Fraunces** (display), **Gelasio** (text), and **IBM Plex Mono** (data & equations), carried forward from the Kronos editorial design system.

The figures are rendered at 300 dpi from the deposited generator scripts; the document is composed as a single self-contained file with embedded fonts and imagery, paginated to US Letter, and rendered to PDF through a headless Chromium engine in matched light and dark editions.

Every headline quantity carries an evidence class; withdrawn and restated values are marked as such. Nothing herein is frozen beyond the founder-approved Tier-A set.

Explore it live — turn the interactive 3-D model, run the deposited solvers in the physics validator, and watch the companion film series.

LEGAL NOTICE

# Notice, status, and distribution

**Conceptual design & simulation study.** This document reports a conceptual design and simulation study. It is not a construction commitment, a safety-analysis report, a regulatory filing, or an offer of securities. Forward-looking statements — schedules, costs, market sizes, and performance — are estimates subject to the limitations set out in the Simulations part and may change.

**Numbers and their classes.** Quantities are reported with evidence classes and case labels; modelled, assumed, and requirement-class values are identified as such and are not to be quoted without their labels.

**Public edition.** This edition carries the physics and design only; all financial, funding, and defense-commercial content has been removed for public distribution. The scientific text corresponds to the arXiv and journal submissions.

THE 2026 KRONOS SERIES

# One programme, many papers

This editorial is one paper in the Kronos 2026 series — a real fusion company's complete, reproducible physics record for a spherical-tokamak breeder and its low-neutron D–$^{3}$He tandem-mirror burners. Every headline number is a frozen anchor in the Physics De-Risking Register.

Explore the whole programme: the De-Risking Register, the interactive 3-D model, and the physics validator.

KRONOS FUSION ENERGY

# *First-Principles Near-Neutral Low-Activation Refractory Alloys for Fusion Plasma-Facing Components: Formation-Energy Screening and Entropy-Stabilized Composition-of-Matter Design*

A real fusion company building real machines. Explore the science, live.

Zenodo · doi:10.5281/zenodo.22645744

Read on kronosfusionenergy.com

The Physics De-Risking Register

 